Supplementary Information: Floquet Engineering in Quantum Chains

D.M. Kennes,[1] A. de la Torre,[2,3] A. Ron,[2,3] D. Hsieh,[2,3] and A.J. Millis[1,4]

[1] *Department of Physics, Columbia University, New York, NY 10027, USA*
[2] *Department of Physics, California Institute of Technology, Pasadena, CA 91125, USA*
[3] *Institute for Quantum Information and Matter, California Institute of Technology, Pasadena, CA 91125, USA*
[4] *Center for Computational Quantum Physics, The Flatiron Institute, New York, NY 10010, USA*

(Dated: February 24, 2018)

SI: HEATING IN REGIME (A)

Fig. S1 shows the entanglement entropy defined by $\mathrm{EE} = -\rho_\mathrm{L} \log(\rho_\mathrm{L})$, where ρ_L is the left half of our infinite system (upper left and right as well as lower left panel). The lower right panel shows the bond-dimension χ (keeping a fixed discarded weight of 10^{-8}). We concentrate on regime (a1) in which we tune a LL, but the other regimes look qualitatively similar. We find that entanglement growth (and with it heating) is suppressed entirely in the regime of high frequency and not to strong fields. In these regimes the value of τ has only a minor effect on the entanglement growth as can be seen by the parallel shifted curves in the lower right panel of Fig. S1.

SI: TUNING A LL

In Fig. S2 the time averaged results at large times ($Jt > 100$) of the momentum dependent correlation function are compared to the ground state prediction employing the effective (Magnus) Hamiltonian with $J \to J^\mathrm{eff} = J_0(E_0/\Omega)J$. Very low momentum as well as momentum very close to π are difficult to extract faithfully, because we employ a Fourier transform over a finite number of lattice sites, with the maximum of $j = 100$.

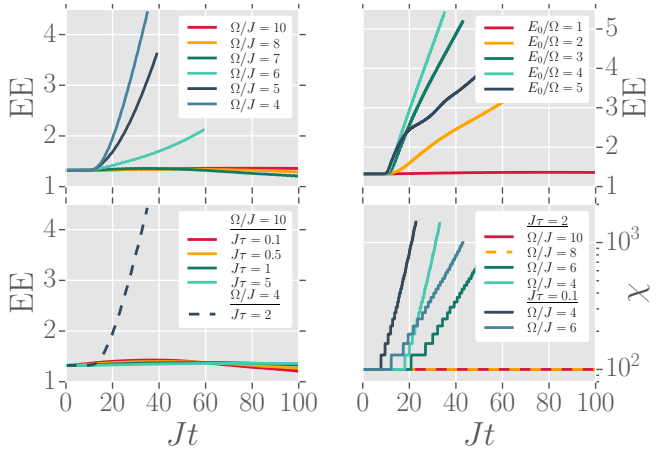

FIG. S1. Entanglement entropy (EE) for the periodically driven system in dependency of Ω (upper left), E_0 (upper right), τ (lower left) as well as the bond-dimension χ (keeping a fixed discarded weight of 10^{-8}) in dependency of both τ and Ω (lower right). The other parameters are $U/J = 0.5$, $\Omega/J = 10$, $E_0/\Omega = 1$, $J\tau = 2$ and $T/J = 0$ if not stated otherwise in the legends.

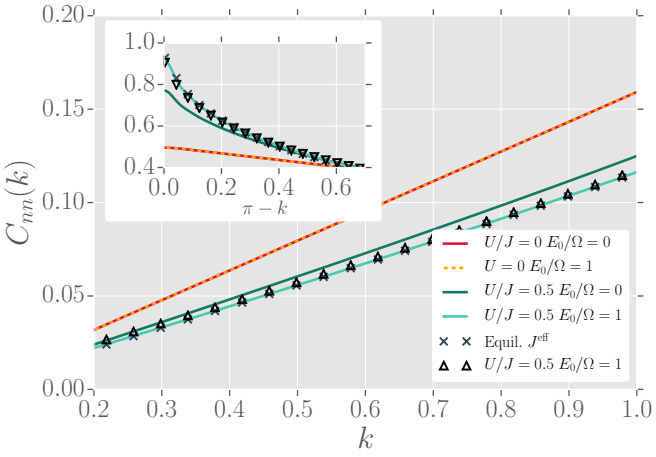

FIG. S2. Time-averaged density-density correlation function $C_{nn}(k)$ (lines and triangles) in momentum space. The other parameters are $J\tau = 2$ (lines) and $J\tau = 0.1$ (triangle), $\Omega/J = 10$ and $T/J = 0$. The $T = 0$ equilibrium prediction for the effective (Magnus) Hamiltonian (crosses) with $J \to J^\mathrm{eff} = J_0(E_0/\Omega)J$ compares well to the time averaged results. Main panel: low momentum behavior $k \to 0$, inset: high momentum behavior $k \to \pi^-$.

The equilibrium properties of the LL phase in our spinless model are characterized by the velocity $v = J\frac{\pi \sin(2\eta)}{2(\pi - 2\eta)}$ as well as the so-called Luttinger Liquid parameter $K = \frac{\pi}{4\eta}$, where $2\eta = \arccos\left(-\frac{U}{J}\right)$. Both v and K depend on the ratio of U/J, which is tuned effectively by the drive in the high frequency regime via tuning $J \to J^\mathrm{eff} = J_0(E_0/\Omega)J$. A hallmark characteristic of LL behavior can be found in the density-density correlations

$$C_{nn}(j) = \left\langle (n_0 - \frac{1}{2})(n_j - \frac{1}{2}) \right\rangle = \frac{K}{2\pi^2 j^2} + C(-1)^j \left(\frac{1}{j}\right)^{2K}, \quad (1)$$

which sensitively depend on K. At low momentum $k \to 0$

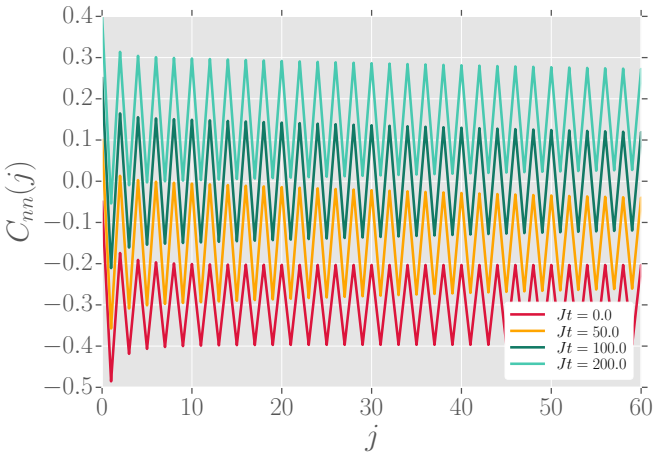

FIG. S3. The correlation function $C_{nn}(j)$ at different times averaged over one drive period. Lines are shifted vertically for clarity of depiction; the midpoint of the oscillation is zero. The parameters are $U/J = 1.7$, $E_0/\Omega = 1.5$ $J\tau = 2$and $T/J = 0$.

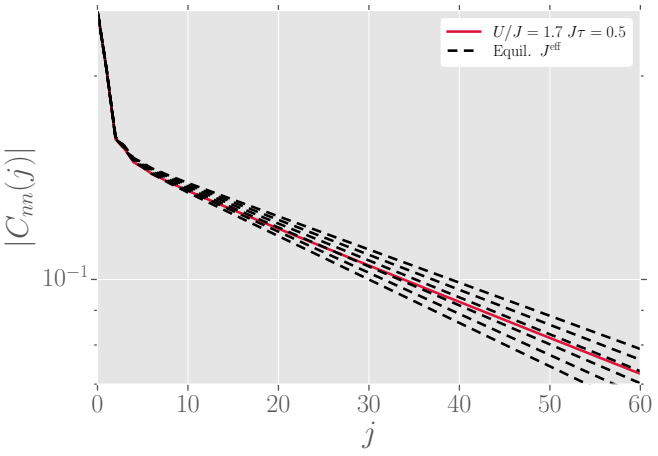

FIG. S4. Time-averaged density-density correlation function $C_{nn}(j)$ for $U/J = 1.7$ and $J\tau = 0.5$ (solid line) compared to different thermal expectations obtained in the Magnus formalism. From bottom to top the temperatures of the thermal expectations are $J/T = 11, 11.2, 11.4, 11.6, 11.8, 12.0$.

this Fourier transforms to

$$C_{nn}(k) \overset{k\to 0}{\longrightarrow} \frac{K}{2\pi}k, \tag{2}$$

while at momentum approaching $k \to \pi^-$ the correlations follow a power-law divergence

$$C_{nn}(k) \overset{k\to\pi^-}{\longrightarrow} (\pi - k)^{2K-2}. \tag{3}$$

We find an unexpected level of agreement of the time averaged results obtained for the periodically driven system and the equilibrium results in the ground state with the appropriate modification $J \to J^{\text{eff}} = J_0(E_0/\Omega)J$, even at very fast ramps of the driving downto $\tau = 0.1$. This is fascinating as quenches in LLs generically lead to faster entanglement growth and the time-scales accessible here are out of reach of DMRG simulations. This means that surprisingly the driving protocol maps the initial ground state more faithfully to the ground state of the effective (time-averaged) model than the quench does, even for very fast ramps of the driving protocol. The reduction in entanglement growth (as indicated already by the reachable time-scales) and heating might provide an intriguing shortcut to adiabatic state preparation in LLs. The two physical protocols of fast ramp of periodic driving and the quench are only formally equivalent if $\tau \ll 1/\Omega$. As indicated here this allows to use fast ramps $J\tau = 0.1$, without introducing large excitation energy in the picture of the effective Hamiltonian (if the frequency is sufficiently large).

SI: TUNING A CDW

In Fig. S3 we show the correlation function $C_{nn}(j)$ at different times averaged over one drive period. The curves for $Jt = 100$ and $Jt = 200$ are stationary on the scale of the plot.

SI: EFFECTIVE TEMPERATURE FITS

In the main text we discussed that using a thermal ensemble within the Magnus formalism captures the exponential decay in the density-density correlation function found in the driven system. However, the functional form of these correlations deviate between the driven case and the thermal equilibrium ensemble. To exemplify this point we show one curve obtained for driving the system compared to the thermal expectations using the Magnus formalism and varying T in Fig. S4. A satisfactory level of agreement can either be obtained at small j but then the slope of exponential decay is not well captured and deviations show up at larger j or the slope of the exponential decay can be fitted well, but then the deviations at small j lead to a parallel offset even at large j.

Next we estimate the form of the effective temperature in this case. Modifying the hopping effectively to smaller values further stabilizes the CDW phase and the gap Δ as well as the asymptotic value of the correlations $\lim_{j\to\infty} C_{nn}(j) = (-1)^j C^{\infty}_{nn}$, rise. We show the time averaged real space correlations $C_{nn}(j)$ compared to the equilibrium prediction for $J \to J^{\text{eff}}$ in Fig 3 of the main plot. The finite speed of the ramp does lead to an, approximately exponential, decay depending on τ in the long range correlations after the ramp. This decay looks qualitatively similar to results obtained at finite temperature, for which the rate of the exponential decay of the correlations at large j scales with T (only at $T = 0$ one obtains strictly long ranged correlations in equilibrium). Although the decay looks exponential,

we emphasize here, that comparing the correlation function for the entire range of j to thermal expectations using the effective Hamiltonian $J \to J^{\text{eff}}$ gives a poor fit (as expected for integrable systems) for any value of T, because one can only either fit well the tail with the right exponential decay at large j or fit well the small j behavior (see above). In the following, we neglect the details at small j and define an effective temperature using the effective Hamiltonian $J \to J^{\text{eff}}$ only by fitting to the asymptotic decay at large j (shown for one example as circles in Fig. 3). This yields a scaling of the effective temperature as shown in the inset of Fig. 3 for the two values of U shown in the main panel. At large values of U, we estimate the amount of energy injected into the system, by relating the Fourier transform of the ramp envelope $\sim \tau/\sinh\left[(\pi\tau\omega)/2\right]$ to the gap. If we set the value of the gap to be Δ (calculated from J and U), the energy injected in the system (which is proportional to the temperature) should follow the general form $T^{\text{eff}}/\Delta^{\text{eff}} = a\Delta\tau\sinh\left(b\tau\Delta\right)$, with a and b unknown proportionality constants. Here Δ^{eff} and Δ are determined from U/J^{eff} and U/J, respectively. Indeed such a behavior is found to agree well with the numerically extracted effective temperatures for large $U/J = 4$ (see dashed line in inset).

SI: TIME EVOLUTION OF PHASE-SLIP

In this section we analyze the dynamics of phaseslips as introduced when effectively ramping across the quantum critical point in more detail. Fig S5(a) exemplifies the concept of a phase slip in the CDW pattern by displaying + and − correlations as up- and down-spins. To highlight the dynamics of phase-slips we introduce the variable ϕ, which is 1 if the CDW pattern has sign which follows the regular (equilibrium) pattern and -1 if not. The likelihood λ of a phase slip to occur scales with the excitation energy acquired by the system through the ramp. In a quasi-classical picture the probability to encounter n phase slips by the time one reached the jth site is given by a binomial distribution $P_n(j) = \binom{j}{n}\lambda^j(1-\lambda)^{j-n}$. Therefore, the smaller the excitation energy the further in j the phase slips are expected to occur as $P_1(j) > P_0(j) \Rightarrow j > j_c$, with $j_c = \frac{1-\lambda}{\lambda}$. Indeed for small excitation energies, the phase slips seem to be beyond the window of $j \leq 100$ we calculated, see Fig S5(b). However, for increasing the amplitude of the drive field (Fig S5(c-e)) the phase slips occur well within the region of $j \leq 100$. Also for smoother ramps (longer τ, less excitation energy, smaller λ) the phase slip thus should move to larger values of j, which is confirmed by our numerics (see supplementary information). A rough estimate relates the position of the first to the second phase slip (phase and anti-phaseslip pair) by a factor of two at small λ, because the region where one expects a single phase slip to occur is roughly given by $P_1(j) > P_0(j)$ and simultaneously $P_1(j) > P_2(j)$, which for small values of λ yields $2j_c > j > j_c$. Our numerics (compare Fig S5(c-e)) are roughly consistent with this predictions before the phaseslip – anti-phaseslip pair starts to attract and eventually annihilates into spin-waves. The attraction of this pair can be studied in a quasi-particle picture, where the phaseslip and anti-phaseslip pair take the role of particles with $\log(r)$ attractive potential. Because we expect the long-time dynamics of these pairs to be overdamped the simple equation of motion of the relative coordinate for the phaseslip pair is given by $\dot{r}(t) = C/r(t)$, where C is a constant describing the ratio of the prefactor of the attractive potential and the viscosity of the phase slips' dynamics. The resulting dynamics read $r(t) = r_0\sqrt{2C(t_0 - t)}$, which is valid for times smaller than the time t_0, where the pair comes very close to each other and annihilates by emitting spin-waves. This rough estimate of the dynamics of the phase-slip anti-phaseslip pair is in reasonable agreement with the numerics as shown as a long-dashed line in Fig S5(d). Additionally, we report that the frequency Ω can be used to effectively tune the constant C controlling the attraction felt by the phaseslip anti-phaseslip pair, with the limit $\Omega \to \infty$ restoring the result of a ramp in J, as expected by a leading order Magnus expansion.

Fig. S6 shows the density-density correlations $C_{nn}(j)$ averaged over the micromotion as a false color plot utilizing a diverging color scheme (white is zero, to highlight the dynamics of the phase slip). As τ is increased (less excitation energy is injected into the system), the phaseslip–antiphaseslip pair is created at larger values of j in accordance to the simple model discussed in the main text (compare left panels in Fig. S6). Tuning Ω one can control the time scales on which the phaseslip pair is annealed out, which means one can tune their effective attraction (compare right panels in Fig. S6). The weak dependence of the results on τ is in agreement with the recent study Ref. [1].

Fig S7 depicts the consequences of the presence of phaseslips for the Fourier transform $C_{nn}(k)$ of the correlation function $C_{nn}(j)$. We show $C_{nn}(k)$ before, during and after the phaseslip has occurred. The consequences of phase-slips for the Fourier transform $C_{nn}(k)$, which we calculate over a finite region in space $j < 100$ are quite severe. The equilibrium $T = 0$ expectation using the effective Hamiltonian from a Magnus expansion would show a pronounced singularity at π, which (for our finite Fourier transform) shows up as a strong feature plus Gibbs ringing at this momentum. In comparison to that the time evolved correlation functions show a strongly suppressed feature, with a maximum that shifts slightly as the phaseslip pair is created. At the time the phaseslips anneal out the maximum shifts back and starts to grow again.

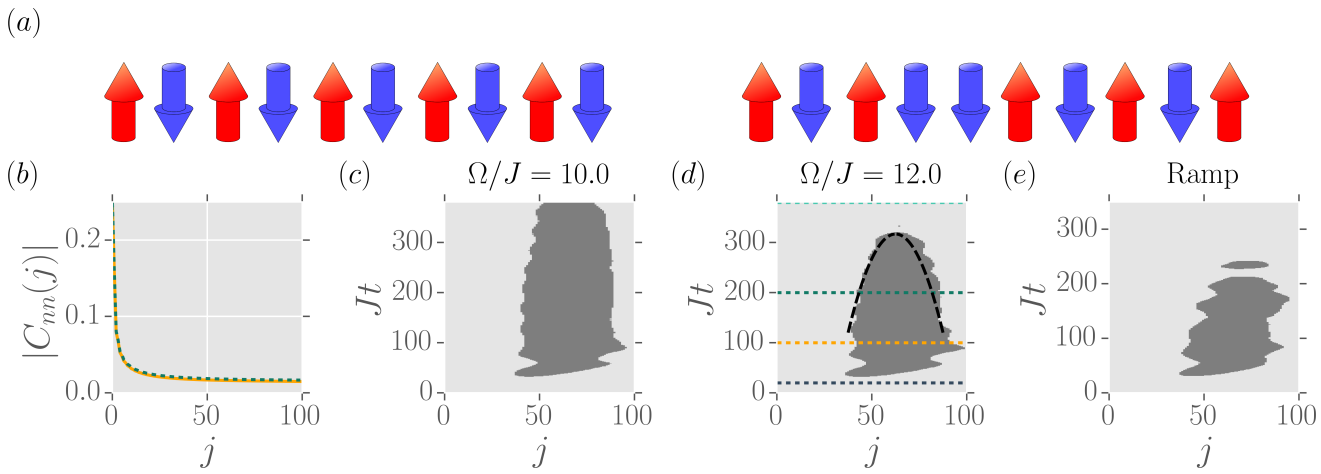

FIG. S5. (a) Depiction of a phase slip, where positive correlations are depicted by an "up spin" and negative correlations by a "down spin". Left: regular CDW pattern. Right: one phase slip between the forth and fifth "spin". (b) Time-averaged correlation function $C_{nn}(j)$ for $U/J = 0.95 < 1$ and $E_0/\Omega = 1$ (solid line) compared to the equilibrium prediction (dashed line) with $J \to J^{\text{eff}} = J_0(E_0/\Omega)J$ (such that $U/J^{\text{eff}} > 1$). The other parameters are $J\tau = 4$, $\Omega/J = 10$ and $T/J = 0$. (c) and (d) time evolution of the phase $\phi(t, j)$ averaged over the micro motion for two values of Ω. Light and dark gray denote the phase of $+1$ and -1, respectively. (e) the same as (c) and (d) but instead driving with a ramp of the hopping following $J(t) = J + (J^{\text{eff}} - J)\left[\frac{1}{2} + \frac{1}{2}\tanh\left(\frac{t}{\tau}\right)\right]$. The other parameters in (c)-(e) are $U/J = 0.95$, $E_0/\Omega = 1.5$ $J\tau = 4$and $T/J = 0$. In (d) we also show the time evolution predicted by a simple model of the dynamics of the phase slips (see text) and include as horizontal lines of the same color the times at which the correlation function i shown in the main text.

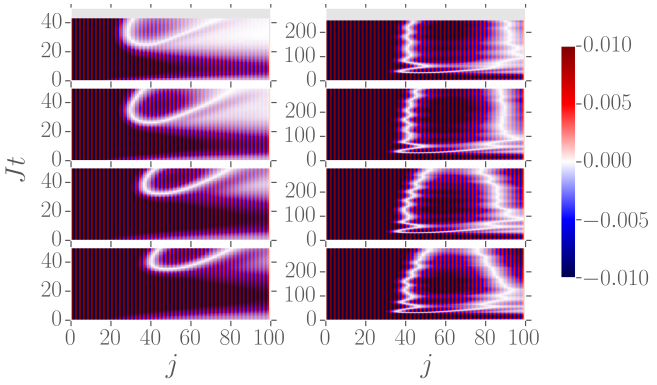

FIG. S6. False color plot of the density-density correlations $C_{nn}(j)$ averaged over the micromotion on a diverging color scale (white is zero) which resolves small absolute values. The other parameters are $U/J = 0.95$, $E_0/\Omega = 1.5$ and $T/J = 0$ as well as $\Omega/J = 10$ for the left panels and $J\tau = 4$ for the right panels. The left panels show $J\tau = 1, 2, 4, 5$ and the right panels show $\Omega/J = 8, 10, 12, 14$ from top to bottom.

SI: HEATING IN REGIME (B)

In Fig. S8 we show the effective hopping J^{eff} following Eq. (3) as a false color plot using a diverging color scheme (white is one). The non-monotonic nature in which J^{eff} can be controlled results in blue and red regions corresponding to effectively increasing or decreasing the hopping by the external drive. We concentrate on $\Omega/U > 0.5$ where resonances are avoided and indicate by semi-transparent or solid blacked out regions the parameter space which leads to heating, and consequently entanglement growth.

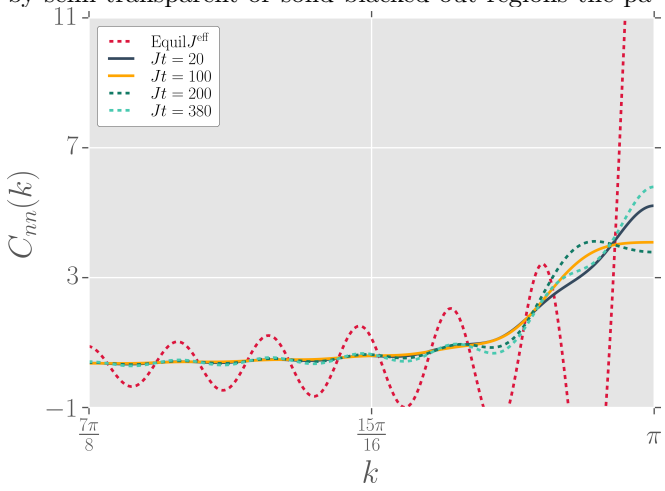

FIG. S7. Fourier transforms of the $C_{nn}(j)$ shown in Fig 5 as well as the ground state prediction for comparison. The other parameters are $J\tau = 4$, $\Omega/J = 12$, $U/J = 0.95$, $E_0/\Omega = 1.5$ and $T/J = 0$.

[1] B. Gardas, J. Dziarmaga, and W. H. Zurek, Phys. Rev. B **95**, 104306 (2017).

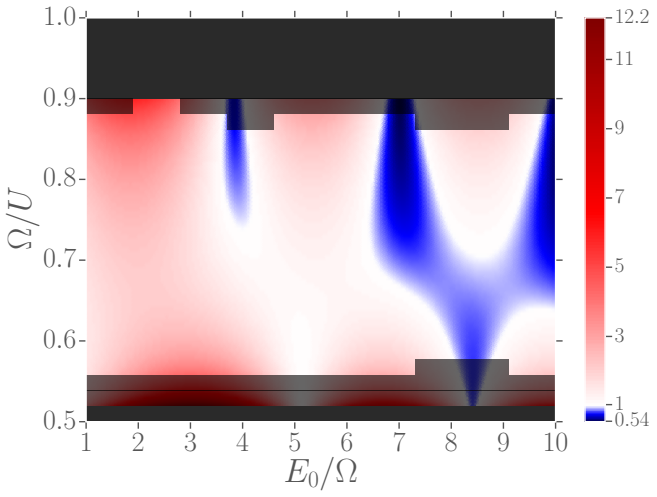

FIG. S8. False color plot of the effective hopping J^{eff} following Eq. (3) using a diverging color scheme (white is one). We block out regions where heating becomes important and large enough time scales to analyze the dynamics cannot be accessed by DMRG, due to entanglement growth. Dark blacked out regions show a much stronger heating rate than semi-transparent blocked out regions.